

Computation of Energy Absorption and Residual Voltage in Metal Oxide Surge Arrester from Digital Models and Lab Tests: A Comparative Study

G. R. S. Lira, D. Fernandes Jr., *Member, IEEE*, and E. G. Costa, *Member, IEEE*

Abstract-- In this work, analysis of some Metal Oxide Surge Arresters (MOSA) models, proposed in literature, were carried out to compare the absorbed energy computed by digital simulations with the energy obtained from laboratory measurements. The residual voltage was compared as well. In digital simulations, it was used the conventional model (nonlinear resistor from ATP), and two frequency-dependent models (IEEE model and the simplified model proposed by Pinceti). In the lab tests, the varistor blocks were submitted to voltage at power frequency, lightning current impulses (8/20 μ s waveform) and fast transients. The voltage and current signals applied to the varistor were recorded and used as the input sources to obtain the digital simulations. As a result, all the models presented good agreement between peak values of voltages for digital simulations and lab. With respect to energy absorption, the models have also shown good agreement results for lightning current impulses. The frequency-dependent models have shown reasonable agreement for fast transients.

Keywords: EMTP, energy absorption, surge arrester, surge arrester models, transient simulations.

I. INTRODUCTION

THE main function of metal oxide surge arresters (MOSA) is to protect transmission and distribution equipments from overvoltages and to absorb electrical energy resulting from lightning or switching surges. Normally, the MOSA are connected between the transmission line and the ground.

Constructively, the MOSA has a simple structure, comprising one or more columns of cylindrical blocks varistors. They present a nonlinear voltage-current characteristic, a high capacity of energy absorption and a strong dependence with the temperature.

In this work, analysis of some MOSA models, proposed in literature, were carried out to compare the residual voltage and the absorbed energy computed by digital simulations with the energy obtained from laboratory measurements. The accuracy of these models becomes very important regarding the

The work was supported by the Brazilian National Research Council (CNPq). G. R. S. Lira is M. Sc. student at Federal University of Campina Grande, 58.109-970, Campina Grande, PB, Brazil (e-mail: georgelira@dee.ufcg.edu.br).

D. Fernandes Jr. and E. G. Costa are with Federal University of Campina Grande, 58.109-970, Campina Grande, PB, Brazil (e-mails: damasio@dee.ufcg.edu.br, edson@dee.ufcg.edu.br).

Presented at the International Conference on Power Systems Transients (IPST'07) in Lyon, France on June 4-7, 2007

application of insulation coordination studies, selection of surge arresters and evaluation of failure probability.

In digital simulations, it has been used the conventional model with a nonlinear resistor (model Type-92 from ATP – Alternative Transients Program [1]), and two frequency-dependent models, (IEEE model proposed by the Working Group 3.4.11 [2] and the simplified model proposed in [3]) due to the surge-arrester dynamic characteristics. In the lab tests, the varistor blocks were submitted to voltage at power frequency (60 Hz), lightning current impulses (8/20 μ s waveform) and fast transients, in order to analyze the behavior of the varistors in the steady-state and under fast transients. These lab tests were made according to [4]. The voltage and current signals applied to the varistor were recorded and used as the input sources to obtain the digital simulations.

In order to determine the absorbed energy and the residual voltage, the values of voltage, current and time were obtained from the measurements and digital simulations.

As a result, all the models (except the conventional model for the fast front surges) presented a good agreement between peak values of voltages for digital simulations and lab tests. About the energy absorption, the results of the models are in good agreement for lightning current impulses. The frequency-dependent models have been reasonable agreement for fast transients.

II. LABORATORY MEASUREMENTS

In lab tests three different ZnO (Zinc-Oxide) varistores were used. Varistor 1 and varistor 2 have diameter equal to 0.0383 m and 0.0458 m of height, each one, and 7.5 kV of rated voltage, while the varistor 3 has 0.0425 m of diameter and 0.0286 m of height, and 4 kV of rated voltage. Measurements to estimate the varistor nonlinear $V - I$ characteristics and to compute the absorbed energy were carried out.

The first linear $V - I$ region (low current region) was obtained at room temperature. The Fig. 1 shows the experimental arrangement to estimate the first linear region. A resistance of 282 k Ω was used to limit the current in cases of short-circuit. A capacitive divider was used to measure the voltages applied to the varistor. The current signal was obtained from a shunt resistance (R_{shunt}). The voltage signals were recorded using a digital oscilloscope and the data saved in a microcomputer. The data acquisition system was developed using a MATLAB [5] routine.

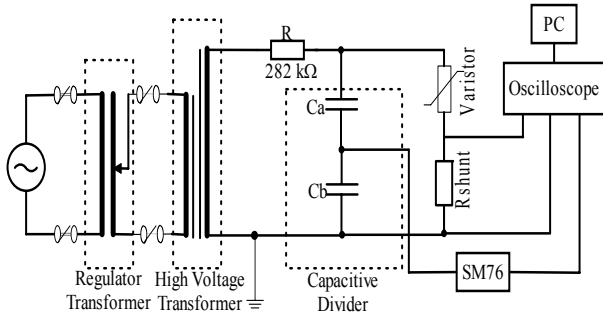


Fig. 1. Experimental arrangement to estimate the first linear region for the varistor $V - I$ characteristic.

The voltage and current waveforms used to estimate the varistor highly nonlinear $V - I$ characteristic were obtained according to the arrangement shown in Fig. 2. This circuit can supply double exponential currents with different waveforms by changing the parameters R , L and C . Initially, the circuit was arranged to submit the varistor to current impulse with 8/20 μ s waveform. The voltage waveform is obtained from the mixed divider and the current waveform is obtained from a shunt resistance ($R_{shunt} = 10.54 \text{ m}\Omega$). The data of voltage and current are saved in the computer using the developed acquisition system.

Following, the parameters R , L and C of the circuit shown in Fig. 2, were changed adequately, to produce a current impulse with 1/10 μ s waveform (fast front surge). Again, the data of voltage and current are saved in the computer using the developed acquisition system.

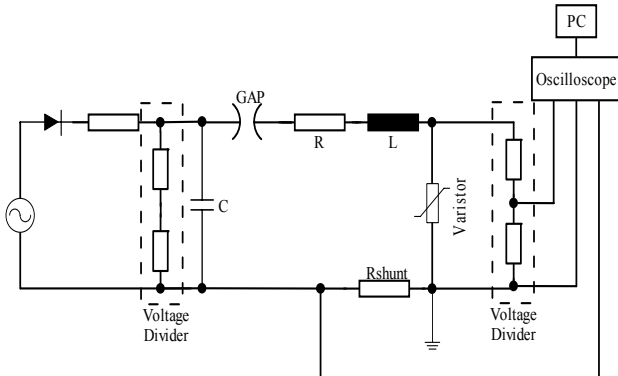


Fig. 2. Experimental arrangement to estimate the highly nonlinear region for the varistor $V - I$ characteristic.

In order to compute the absorbed energy by the ZnO varistor, it was used the trapezoidal rule:

$$E = \int_0^{t_f} v(t)i(t)dt \cong \sum_{j=1}^{n-1} \left[0.5h(V_j I_j + V_{j+1} I_{j+1}) \right] \quad (1)$$

where, $v(t)$ and $i(t)$ are the instantaneous voltage and current across the varistor, respectively, V_j and I_j are the sampled instantaneous voltage and current, n is the number of samples and h is the time-step for computation. The values of V_j and I_j were obtained from the tests, whose arrangements are shown in Figs. 1 and 2.

The data points for nonlinear characteristic curves of the varistors 1, 2 and 3 are shown in Table I.

TABLE I
DATA POINTS FOR THE NONLINEAR CHARACTERISTIC CURVES FOR THE VARISTORS 1, 2 AND 3.

Varistor 1		Varistor 2		Varistor 3	
I (A)	V (kV)	I (A)	V (kV)	I (A)	V (kV)
$7.7 \cdot 10^{-4}$	$1.1 \cdot 10^3$	$9.6 \cdot 10^{-4}$	$9.7 \cdot 10^2$	$1.3 \cdot 10^{-3}$	$7.8 \cdot 10^2$
$2.2 \cdot 10^{-3}$	$3.2 \cdot 10^3$	$2.1 \cdot 10^{-3}$	$2.5 \cdot 10^3$	$1.7 \cdot 10^{-3}$	$9.7 \cdot 10^2$
$3.5 \cdot 10^{-3}$	$5.3 \cdot 10^3$	$2.8 \cdot 10^{-3}$	$3.3 \cdot 10^3$	$3.1 \cdot 10^{-3}$	$2.0 \cdot 10^3$
$5.2 \cdot 10^{-3}$	$8.0 \cdot 10^3$	$4.7 \cdot 10^{-3}$	$6.0 \cdot 10^3$	$3.8 \cdot 10^{-3}$	$2.6 \cdot 10^3$
$6.9 \cdot 10^{-3}$	$1.0 \cdot 10^4$	$5.6 \cdot 10^{-3}$	$7.5 \cdot 10^3$	$5.0 \cdot 10^{-3}$	$3.3 \cdot 10^3$
$7.3 \cdot 10^{-3}$	$1.1 \cdot 10^4$	$6.9 \cdot 10^{-3}$	$8.8 \cdot 10^3$	$6.7 \cdot 10^{-3}$	$4.6 \cdot 10^3$
$9.8 \cdot 10^{-3}$	$1.1 \cdot 10^4$	$7.9 \cdot 10^{-3}$	$9.9 \cdot 10^3$	$7.7 \cdot 10^{-3}$	$5.4 \cdot 10^3$
$1.6 \cdot 10^{-2}$	$1.2 \cdot 10^4$	$9.0 \cdot 10^{-3}$	$1.0 \cdot 10^4$	$9.4 \cdot 10^{-3}$	$6.0 \cdot 10^3$
$2.9 \cdot 10^{-2}$	$1.2 \cdot 10^4$	$1.3 \cdot 10^{-2}$	$1.1 \cdot 10^4$	$1.6 \cdot 10^{-2}$	$6.7 \cdot 10^3$
$1.2 \cdot 10^{-1}$	$1.3 \cdot 10^4$	$2.7 \cdot 10^{-2}$	$1.2 \cdot 10^4$	$2.8 \cdot 10^{-2}$	$6.9 \cdot 10^3$
$5.1 \cdot 10^{-3}$	$2.1 \cdot 10^4$	$3.8 \cdot 10^{-2}$	$1.2 \cdot 10^4$	$5.8 \cdot 10^{-2}$	$7.1 \cdot 10^3$
$1.0 \cdot 10^4$	$2.2 \cdot 10^4$	$5.9 \cdot 10^{-2}$	$1.3 \cdot 10^4$	$7.1 \cdot 10^3$	$1.2 \cdot 10^4$
$1.6 \cdot 10^4$	$2.3 \cdot 10^4$	$5.8 \cdot 10^{-3}$	$2.0 \cdot 10^4$	$1.0 \cdot 10^4$	$1.3 \cdot 10^4$
-	-	$1.1 \cdot 10^4$	$2.1 \cdot 10^4$	$1.3 \cdot 10^4$	$1.4 \cdot 10^4$
-	-	$1.4 \cdot 10^4$	$2.2 \cdot 10^4$	-	-

III. SURGE ARRESTER MODELS

A. Conventional Model

In this paper, the surge arrester conventional model was represented by a nonlinear resistor (model Type-92 from ATP). This model provides a true representation of the nonlinearity of the varistor through a piecewise-linear characteristic of current and voltage [1]. The nonlinear resistor is shown in Fig. 3.

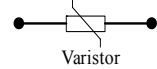


Fig. 3. Conventional surge arrester model: nonlinear resistor (model Type-92 from ATP).

In this model, the dynamic characteristic of the surge arrester is not taken into account. The voltage peak occurs in the same time of current peak, even for current waveforms which the peak is in the range of 8 μ s and faster.

B. The IEEE Model

This model was proposed by the IEEE Working Group 3.4.11 and it is referred to a frequency-dependent model [2]. It is composed by two sections of nonlinear resistance, usually designated by A_0 and A_1 , which are separated by a R-L filter, as shown in Fig. 4. For slow-front surges, the R-L filter has low impedance and the nonlinear resistances A_0 and A_1 are almost in parallel. However, for fast-front surges the impedance of the R-L filter is highest. As consequence of this, the current in nonlinear resistance A_0 increases such as the voltage. Since characteristic A_0 has a higher voltage than A_1 for a given current (as shown in Fig. 5), the result is that the arrester model generates a higher voltage for fast transients (dynamic characteristics of the MOSA).

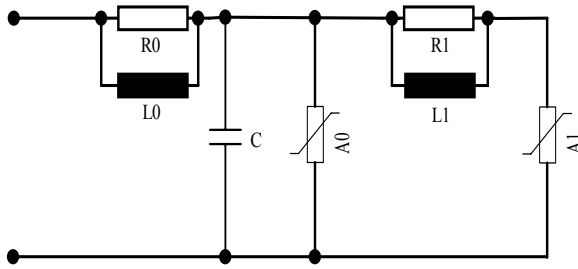


Fig. 4. IEEE surge arrester model.

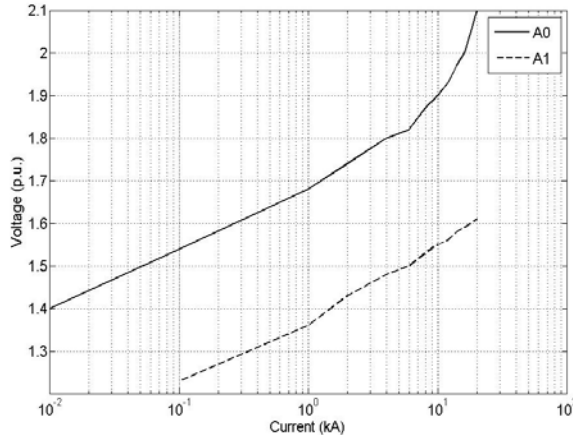


Fig. 5. Characteristic of the nonlinear elements A_0 and A_1 proposed by IEEE Working Group 3.4.11.

In this model, L_0 represents the inductance associated with magnetic field near the arrester. The resistor R_0 is used to avoid numerical instabilities and the capacitance C represents the terminal-to-terminal capacitance of the arrester. These parameters are estimated by (2).

$$\begin{aligned} L_1 &= 15d/n \text{ } (\mu\text{H}) \\ R_1 &= 65d/n \text{ } (\Omega) \\ L_0 &= 0.2d/n \text{ } (\mu\text{H}) \\ R_0 &= 100d/n \text{ } (\Omega) \\ C &= 100n/d \text{ } (\text{pF}) \end{aligned} \quad (2)$$

where:

d is the estimated height of the arrester in meters;

n is the number of parallel columns of metal oxide in the arrester.

After the evaluation of the parameters is necessary to adjust the characteristics A_0 and A_1 , and the parameter L_1 by trial and error procedure, as described in [2], to obtain a good match to the discharge voltages for switching and 8/20 μs discharge currents, respectively.

C. Model Proposed by Pinceti

The model proposed by Pinceti derives from the IEEE model. In this model, the capacitance and the two resistances in parallel with the inductances were eliminated and a resistance R (about 1 $M\Omega$) was added to avoid numerical problems [3]. The proposed circuit is shown in Fig. 6.

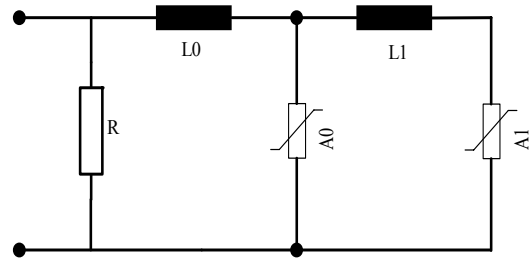


Fig. 6 Surge arrester model proposed by Pinceti.

The most important characteristic of this model is that the parameters are calculated only from electrical data, in opposition to the IEEE model which takes into account physical characteristics of the arrester. The inductances L_0 and L_1 are given by (3).

$$\begin{aligned} L_1 &= \frac{1}{4} \frac{V_{r1/T2} - V_{r8/20}}{V_{r8/20}} V_n \text{ } (\mu\text{H}) \\ L_0 &= \frac{1}{12} \frac{V_{r1/T2} - V_{r8/20}}{V_{r8/20}} V_n \text{ } (\mu\text{H}) \end{aligned} \quad (3)$$

where:

V_r is the arrester rated voltage (kV);

$V_{r1/T2}$ is the residual voltage at 10 kA fast front current surge (kV);

$V_{r8/20}$ is the residual voltage at 10 kA current surge with a 8/20 μs shape (kV).

IV. DIGITAL SIMULATIONS

The described models were implemented in ATP. With these circuits, is possible to simulate the behavior of the surge arrester for voltage at industrial frequency and several surges. The necessary measured data to compute the parameters of the IEEE and Pinceti models are shown in the Tables II, III and IV, respectively, for the varistors 1, 2 and 3.

TABLE II
VARISTOR 1 DATA.

V_r	$V_{r8/20}$ (\approx 10 kA)	$V_{r1/T2}$ (\approx 10 kA)	d – height	n – number of columns
7.5 kV	21557 V	26269 V	0.0458 m	1

TABLE III
VARISTOR 2 DATA.

V_r	$V_{r8/20}$ (\approx 10 kA)	$V_{r1/T2}$ (\approx 10 kA)	d – height	n – number of columns
7.5 kV	20908 V	22824 V	0.0458 m	1

TABLE IV
VARISTOR 3 DATA.

V_r	$V_{r8/20}$ (\approx 10 kA)	$V_{r1/T2}$ (\approx 10 kA)	d – height	n – number of columns
4 kV	13102 V	15059 V	0.0286 m	1

A. Energy Computation at the Operation Voltage

In order to simulate the behavior of surge arrester at the operation voltage was used the conventional model, as shown in Fig. 7.

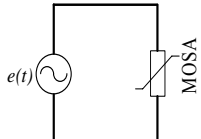


Fig. 7. Model used in digital simulations.

The signal $e(t)$ is a sinusoidal source obtained from the lab measurements. The element MOSA is a piecewise-linear resistance (Type 92) with points of current and voltage obtained from the varistor nonlinear characteristic, shown in Table I. The maximum time of simulation was 50 ms (3 cycles at power frequency), and the simulation time-step was 20 μ s.

The energy is computed according to (1), where, V_j and I_j are the instantaneous values of voltage and current, respectively, obtained from the ATP simulations, n is the number of computed points and h is the simulation time-step.

B. Energy Computation for Current Surges

The energy computation for lightning current impulse and for fast front surge was carried out by the conventional model, IEEE model and Pinceti model. The current signal applied to the varistor were recorded from the measurements and used as input source.

Again, the model shown in Fig. 7 was used in these simulations. The element MOSA was replaced by a piecewise-linear resistance, the IEEE model (Fig. 4) and the Pinceti model (Fig. 6), for the simulations of the three analyzed cases. The signal $e(t)$ represents the current signal. The simulation time was 100 μ s and the simulation time-step was 40 ns, in all of the cases. The energy is computed according to (1), where, V_j and I_j are the instantaneous values of voltage and current, respectively, obtained from the ATP simulations, n is the number of computed points and h is the simulation time-step.

V. ANALYSIS OF RESULTS

The simulated and measured values of residual voltage and absorbed energy by three MOSAs were compared for three different situations: operation voltage, lightning current impulse and fast front surge ($\approx 1/10 \mu$ s).

In Table V is shown the obtained results of the absorbed energy for measurements and simulations when the varistor is operating at power frequency. By the analysis of these results, it is observed divergences between the measured energies and those obtained from the ATP model (conventional model). It occurs due to the delay between current and voltage existent in the measurements (Fig. 8), because the MOSA total current consists of a large capacitive component and a small resistive component [6]. Another reason for the divergence is that there is a distortion in the current waveform due to the third harmonic of the resistive component [7]. These effects are minimized whereas the voltage across the MOSA is increased.

In the conventional model is not represented the “capacitive” behavior of the MOSA. So, the total current is purely resistive (see Fig. 9). Therefore, the energy obtained from the ATP model is large than the energy obtained from measurements.

TABLE V
ABSORBED ENERGY BY THE VARISTORS 1, 2 AND 3 AT POWER FREQUENCY.

Varistor	Peak Voltage	Measured Value	From the ATP Model (Type 92)
1	5292.2 V	0.018 J	0.503 J
2	5963.0 V	0.027 J	0.774 J
3	3316.9 V	0.016 J	0.449 J

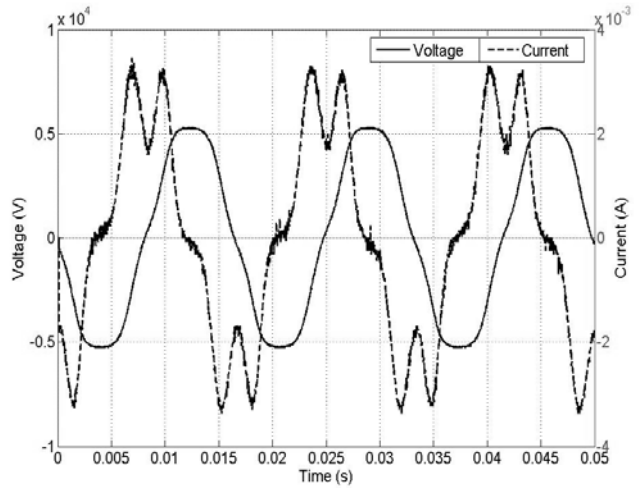


Fig. 8. Voltage and current to the varistor 1 obtained from the measurements.

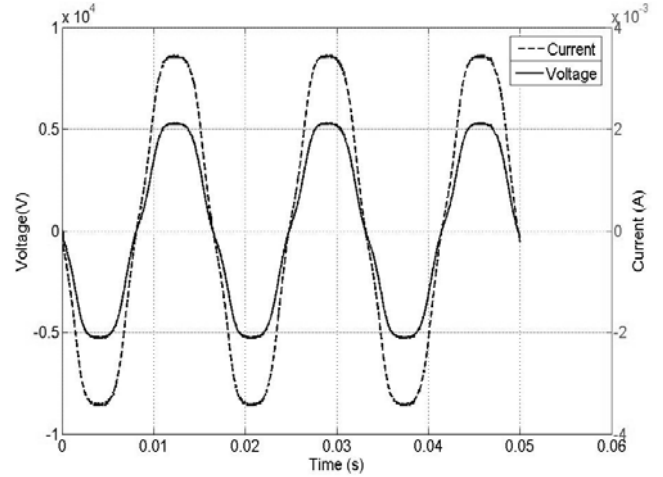


Fig. 9. Voltage and current to the varistor 1 obtained from the ATP.

As shown in Tables VI to XI, in the case of lightning current impulse, the three ATP models (conventional, IEEE and Pinceti) present good results for both residual voltages and absorbed energy whenever compared with the measurements. It occurs because the data points used in the conventional model were obtained from lab tests. Whereas, both IEEE model and the Pinceti model were proposed to work adequately for lightning current impulse situation, thus, good results have already expected.

In spite of the obtained results, two troubles should be outstanding: the iterative process for match the parameters of IEEE model; and numerical oscillation of the Pinceti model.

TABLE VI

ABSORBED ENERGY BY THE VARISTOR 1 FOR LIGHTING CURRENT IMPULSE.

From the measurements

6413.1 J		
From the ATP Model		
Type 92	IEEE	Pinceti
6333.6 J	6497.7 J	6496.6 J
Error (%)		
1.24	-1.32	-1.30

TABLE VII

RESIDUAL VOLTAGE TO THE VARISTOR 1 FOR LIGHTING CURRENT IMPULSE.

From the measurements

21557 V		
From the ATP Model		
Type 92	IEEE	Pinceti
21557 V	21558 V	22059 V
Error (%)		
0.00	$-4.64 \cdot 10^{-3}$	-2.33

TABLE VIII

ABSORBED ENERGY BY THE VARISTOR 2 FOR LIGHTING CURRENT IMPULSE.

From the measurements

6716.4 J		
From the ATP Model		
Type 92	IEEE	Pinceti
6638.6 J	6912.5 J	6911 J
Error (%)		
1.16	-2.92	-2.90

TABLE IX

RESIDUAL VOLTAGE TO THE VARISTOR 2 FOR LIGHTING CURRENT IMPULSE.

From the measurements

20908 V		
From the ATP Model		
Type 92	IEEE	Pinceti
20914 V	20917 V	21104 V
Error (%)		
$-2.87 \cdot 10^{-2}$	$-4.3 \cdot 10^{-2}$	-0.94

TABLE X

ABSORBED ENERGY BY THE VARISTOR 3 FOR LIGHTING CURRENT IMPULSE.

From the measurements

3151.9 J		
From the ATP Model		
Type 92	IEEE	Pinceti
2976.1 J	3201.9 J	3200.9 J
Error (%)		
5.58	-1.59	-1.55

TABLE XI

RESIDUAL VOLTAGE TO THE VARISTOR 3 FOR LIGHTING CURRENT IMPULSE.

From the measurements

13102 V		
From the ATP Model		
Type 92	IEEE	Pinceti
13104 V	13110 V	13287 V
Error (%)		
$-1.53 \cdot 10^{-2}$	$-6.11 \cdot 10^{-2}$	-1.41

The data shown in Tables of XII to XVII is obtained assigning the signal source of the circuit shown in Fig. 7 by a fast front surge obtained from lab tests for each varistor. The frequency-dependent models present good results for residual voltage of the three varistors. Whereas, the Pinceti model presented numerical oscillation and the IEEE model had more consistent results. In the case of energy absorption, the conventional model had the best results. It occurs because the fitting parameters of the frequency-dependent model takes into account only the final value of the residual voltage, i.e., the voltage waveform is neglected. This procedure may result in a good fit of the waveform, but there are cases in which it is not occur. The conventional model does not represent the dynamic characteristics of the MOSA, even so, there are situations in which it has a best fit of the voltage waveform. Consequently, the energy obtained from this model provides best results.

TABLE XII

ABSORBED ENERGY BY THE VARISTOR 1 FOR FAST FRONT SURGE.

From the measurements

3928.4 J		
From the ATP Model		
Type 92	IEEE	Pinceti
3662.3 J	3822 J	3816.9 J
Error (%)		
6.77	2.71	2.84

TABLE XIII

RESIDUAL VOLTAGE TO THE VARISTOR 1 FOR FAST FRONT SURGE.

From the measurements

26269 V		
From the ATP Model		
Type 92	IEEE	Pinceti
21616 V	23410 V	24648 V
Error (%)		
17.71	10.88	6.17

TABLE XIV

ABSORBED ENERGY BY THE VARISTOR 2 FOR FAST FRONT SURGE.

From the measurements

2633.2 J		
From the ATP Model		
Type 92	IEEE	Pinceti
2716.9 J	2917.1 J	2913.6 J
Error (%)		
-3.18	-10.78	-10.65

TABLE XV
RESIDUAL VOLTAGE TO THE VARISTOR 2 FOR FAST FRONT SURGE.
From the measurements

22824 V		
From the ATP Model		
Type 92	IEEE	Pinceti
20528 V	22341 V	22193 V
Error (%)		
10.06	2.12	2.76

TABLE XVI
ABSORBED ENERGY BY THE VARISTOR 3 FOR FAST FRONT SURGE.
From the measurements

1623.7 J		
From the ATP Model		
Type 92	IEEE	Pinceti
1626.6 J	1806.1 J	1802.7 J
Error (%)		
-0.18	-11.23	-11.02

TABLE XVII
RESIDUAL VOLTAGE TO THE VARISTOR 3 FOR FAST FRONT SURGE.
From the measurements

15059 V		
From the ATP Model		
Type 92	IEEE	Pinceti
12994 V	14124 V	14117 V
Error (%)		
13.71	6.21	6.26

VI. CONCLUSIONS

This work has presented a comparative study of three MOSA models: conventional model, IEEE and Pinceti proposed models. It was compared the values of energy absorption and residual voltage obtained from lab tests and ATP simulations. In order to do that, it was considered three types of excitation: operation voltage, lighting current impulse and fast front surge.

The results have shown that the conventional model cannot represent the “capacitive” behavior (only the “resistive” behavior) of the MOSA, which occurs whenever it is excited by a voltage below of the rated voltage. Therefore the results of energy absorption at voltage operation were divergent. The results of energy absorption have shown good accuracy for both lighting current impulse and fast front surge. The values of residual voltages did not have good accuracy for fast front surges like lighting impulse current, because the conventional model does not include the dynamic effects of voltage-current characteristics of the MOSA.

The IEEE and Pinceti proposed models have presented solid results of residual voltage and of energy absorption for lighting current impulse. The values of the absorbed energy for the fast front surge were reasonable, but the values of residual voltage had good accuracy.

VII. ACKNOWLEDGMENT

The authors gratefully acknowledge the contributions of K. M. C. Dantas and K. M. Silva for their work on the original version of this document. The authors are also very grateful to the reviewers for their invaluable suggestions.

VIII. REFERENCES

- [1] Leuven EMTP Center, Alternative Transients Program – Rule Book, Heverlee, Belgium, 1987.
- [2] IEEE Working Group 3.4.11, "Modeling of metal oxide surge arresters," IEEE Trans. on Power Delivery, vol. 7, n° 1, pp. 302-309, Jan. 1992.
- [3] P. Pinceti and M. Giannettoni, "A simplified model for zinc oxide surge arresters," IEEE Trans. on Power Delivery, vol. 14, n° 2, pp. 393-398, Apr. 1999.
- [4] IEC Metal-oxide surge arresters without gaps for a.c. systems, IEC Standard 60099-4, Dec. 2001.
- [5] The Math Works Inc., MATLAB, the Language of Technical Computing, 2000.
- [6] V Hinrichsen, "Metal oxide surge arrester fundamentals". Siemens AG, Berlin - Germany, Jul. 2001.
- [7] H. Zhu and M. R. Raghubeer, "Influence of harmonics in system voltage on metal oxide surge arrester diagnostics," in Proc. 1999 Conference on Electrical Insulation and Dielectric Phenomena, pp. 542-545.

IX. BIOGRAPHIES

George R. S. Lira was born in Brazil in 1980. He received the B.Sc. degree in electrical engineering from Federal University of Campina Grande, Brazil, in 2005. He is M.Sc. student at the Federal University of Campina Grande, Brazil. His research interests are: high voltage, surge arresters, electromagnetic transients and optimization methods for power system applications.

Damásio Fernandes Jr. (M'2005) was born in Brazil in 1973. He received the B.Sc. and M.Sc. degrees in electrical engineering from Federal University of Paraíba, Brazil, in 1997 and 1999, respectively, and the Ph.D. degree in electrical engineering from Federal University of Campina Grande, Brazil, in 2004. Since 2003, he is with the Department of Electrical Engineering of Federal University of Campina Grande. His research interests are electromagnetic transients and optimization methods for power system applications.

Edson G. Costa was born in Brazil in 1954. He received the B.Sc. and M.Sc. degrees in electrical engineering in 1978 and 1981, respectively, and the Ph.D. degree in 1999, all from the Federal University of Paraíba. Since 1978, he has been with the Department of Electrical Engineering, Federal University of Campina Grande, Campina Grande, PB, Brazil. His research interests include high voltage, surge arresters, insulators, partial discharge and electric fields.